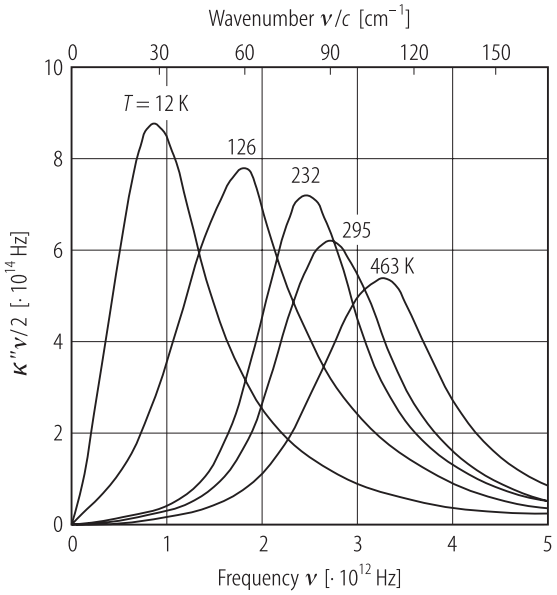

Fig. 1A-5-046. $KTaO_3$. $\kappa'' \nu/2$ vs. ν [67Per]. Parameter: T. κ'' was calculated from the reflectivity data; $\kappa'' \nu/2$ is proportional to the infrared conductivity.

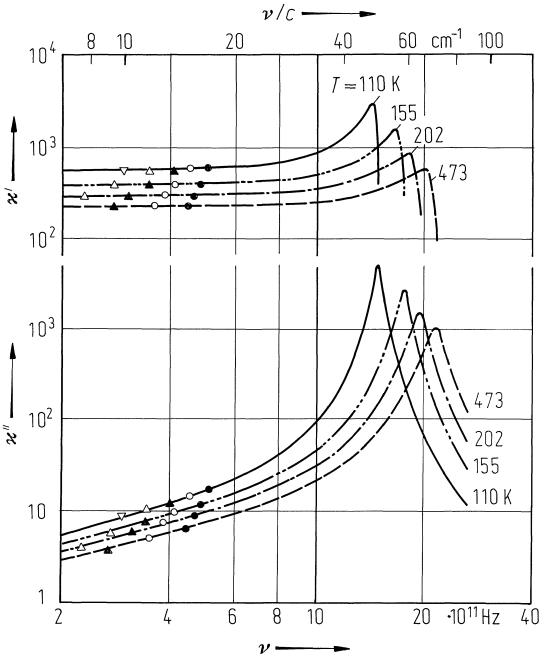

Fig. 1A-5-047. $KTaO_3$. κ', κ'' vs. ν [86Vol]. Parameter: T.

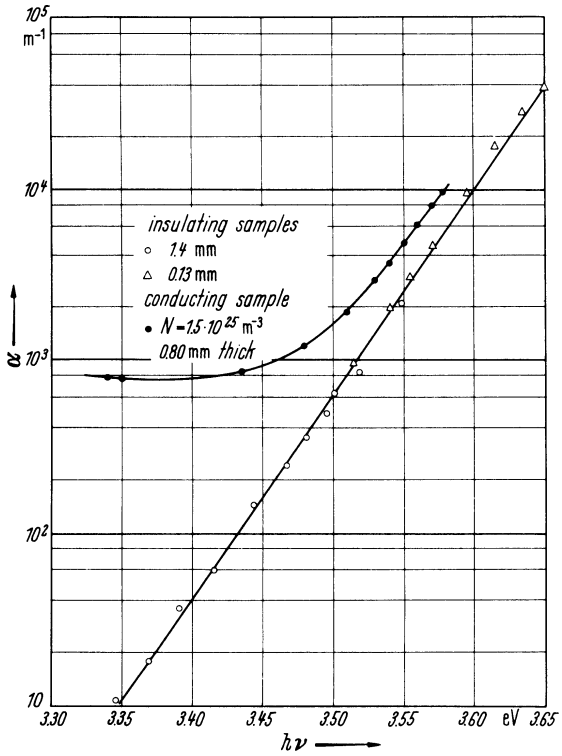

Fig. 1A-5-048. $KTaO_3$. α vs. $h\nu$ near interband edge [65Wem]. α: absorption coefficient. Parameter: carrier concentration N.

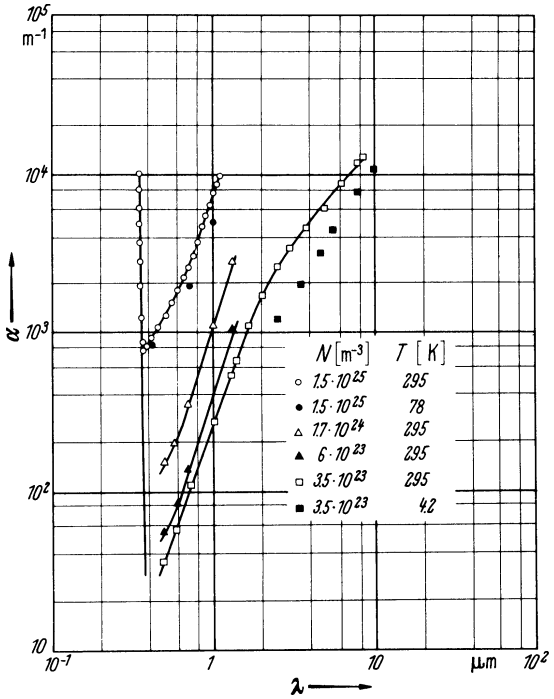

Fig. 1A-5-049. $KTaO_3$. α vs. λ [65Wem]. α: absorption coefficient. Parameter: *T* and carrier concentration *N*.

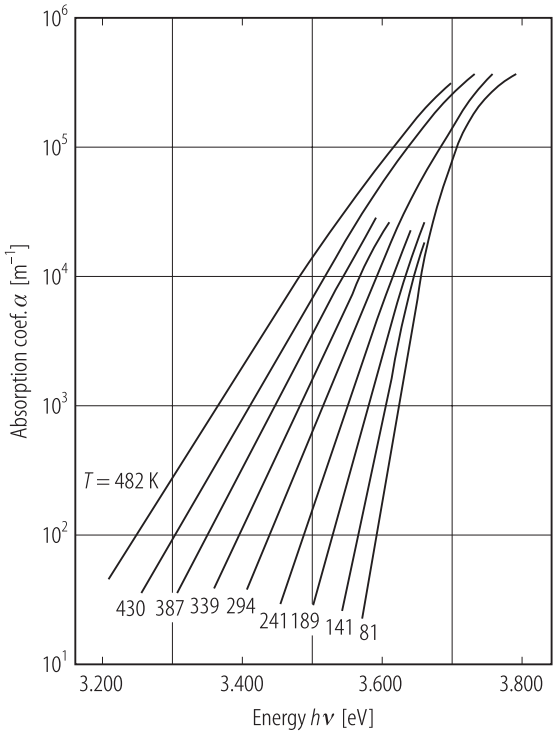

Fig. 1A-5-050. $KTaO_3$. α vs. $h\nu$ [72Cap]. α: absorption coefficient. Parameter: *T*.

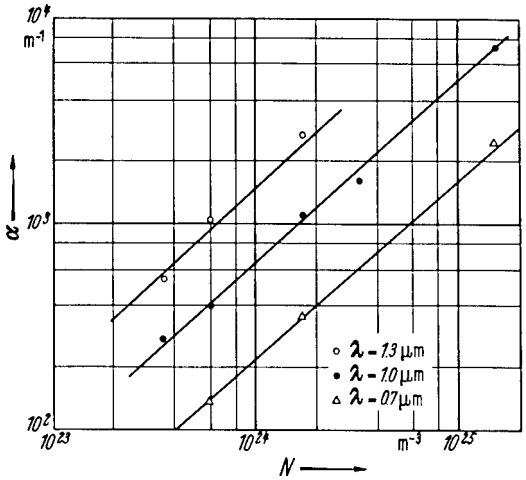

Fig. 1A-5-051. $KTaO_3$. α vs. carrier concentration N [65Wem]. α: absorption coefficient. Parameter: λ.

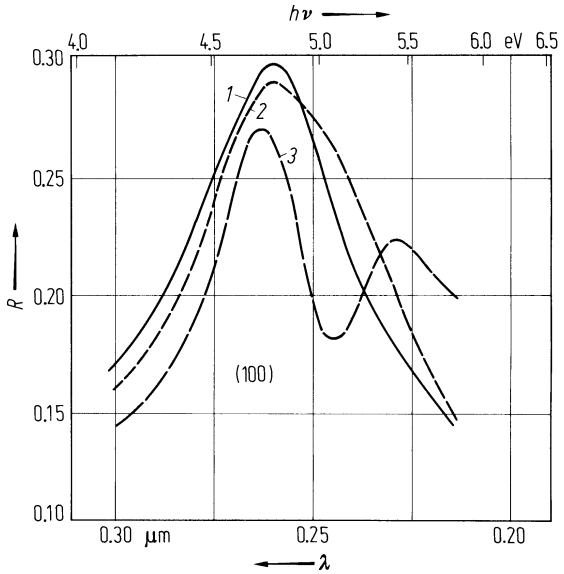

Fig. 1A-5-052. $KTaO_3$. R vs. λ [67Fle]. R: reflectance of (100) surface. Parameter: interface field E. Curve *1*: $E = 3 \cdot 10^7$ Vm^{-1} (no applied field, only an interface barrier field is present); curve *2*: $E = 9 \cdot 10^7$ Vm^{-1}; curve *3*: $E = 2.6 \cdot 10^8$ Vm^{-1}. The semiconducting $KTaO_3$ is immersed in K_2SO_4 aqueous solution.

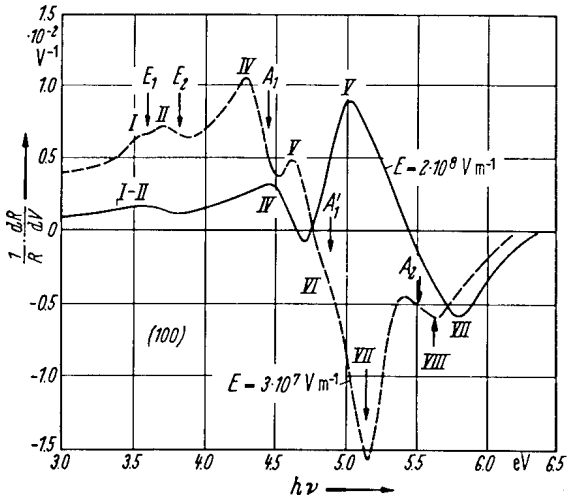

Fig. 1A-5-053. $KTaO_3$ (Ca-doped). $1/R \cdot dR/dV$ vs. $h\nu$ for (100) surface [67Fle]. *R*: reflectance, *V*: applied voltage. Parameter: field strength *E* at the (100) interface. Donor density: $3.8 \cdot 10^{24}$ m^{-3}. E_1, E_2, A_1, A_1', A_2: singularities, see Table 1A-5-002.

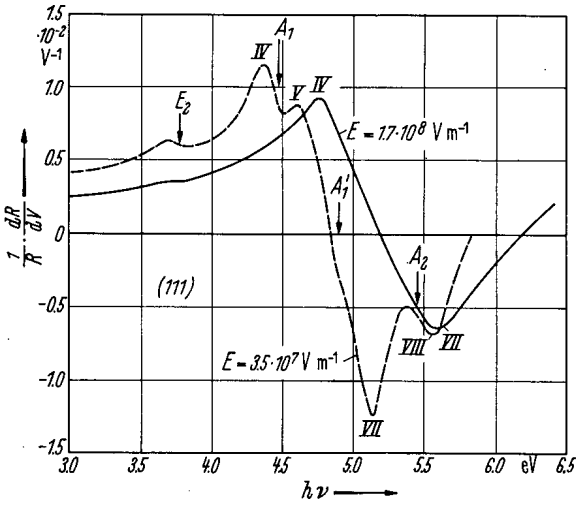

Fig. 1A-5-054. $KTaO_3$ (Ca-doped). $1/R \cdot dR/dV$ vs. $h\nu$ for (111) surface [67Fle]. Parameter: field strength E at the (111) interface. Donor density: $3.5 \cdot 10^{24}$ m^{-3}. See Fig. 1A-5-053, Table 1A-5-002.

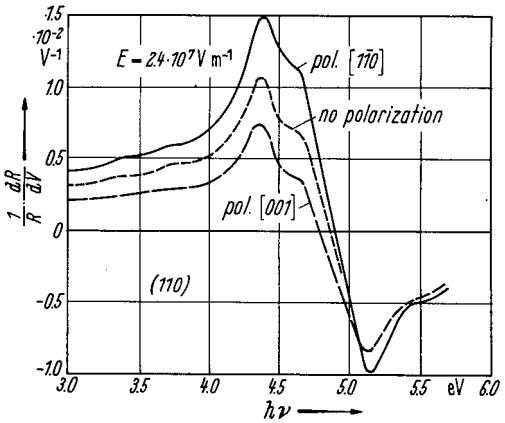

Fig. 1A-5-055. $KTaO_3$ (Ca-doped). $1/R \cdot dR/dV$ vs. $h\nu$ for (110) surface [67Fle]. Parameter: direction of the electric vector of the incident polarized light. Interface field $E = 2.4 \cdot 10^7$ Vm^{-1}.

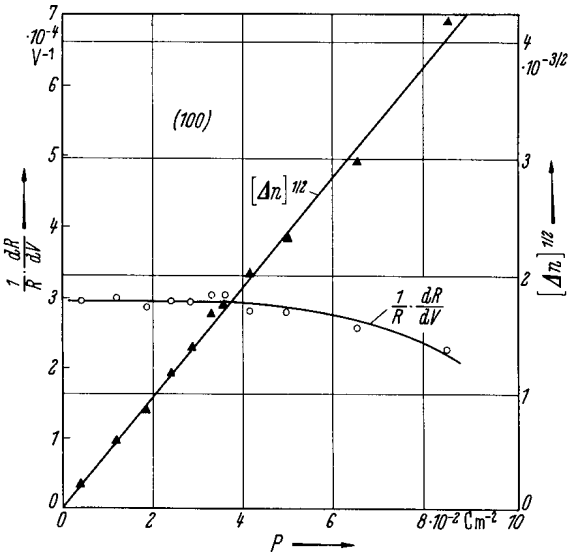

Fig. 1A-5-056. $KTaO_3$ (lightly doped). $1/R \cdot dR/dV$, $(\Delta n)^{1/2}$ vs. P for incident light of photon energy 4 eV [67Fle]. P: dielectric polarization at the (100) surface, Δn: change of the refractive index $\Delta n = n(0) - n(P)$. Donor density: $1.5 \cdot 10^{23}$ m^{-3}.

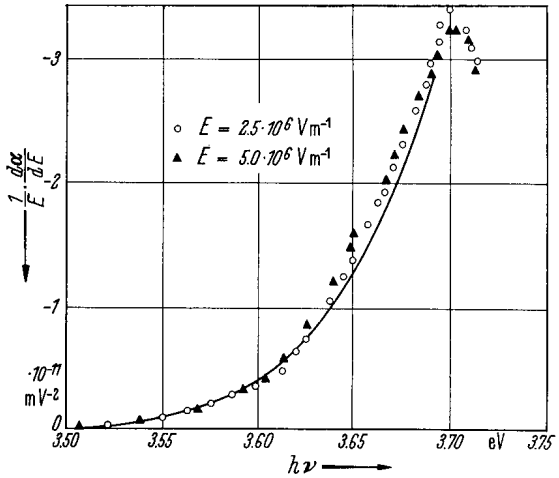

Fig. 1A-5-057. $KTaO_3$. $1/E \cdot d\alpha/dE$ vs. $h\nu$ [67Fle]. α: absorption coefficient. Parameter: electric field E. The solid curve gives the slope of the absorption edge $d\alpha/d(h\nu)$ in arbitary units.

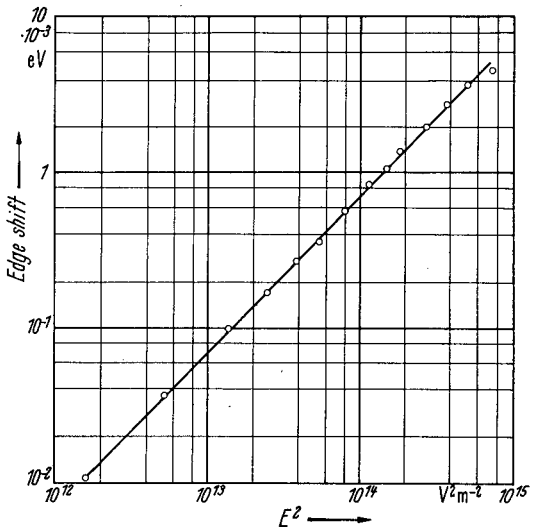

Fig. 1A-5-058. $KTaO_3$. Increase of the fundamental energy gap vs. E^2 [67Fle].

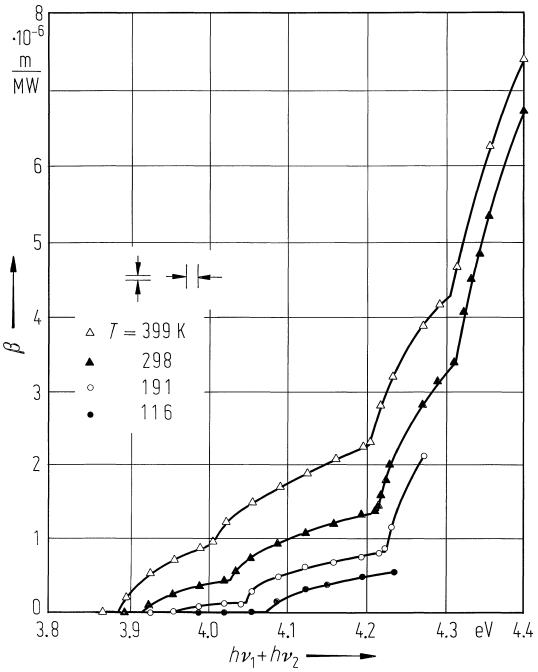

Fig. 1A-5-059. $KTaO_3$. β vs. $h\nu_1+h\nu_2$ [84Sha]. β: Two-phonon absorption coefficient. $h\nu_1$ = 1.17 eV. Parameter: T.

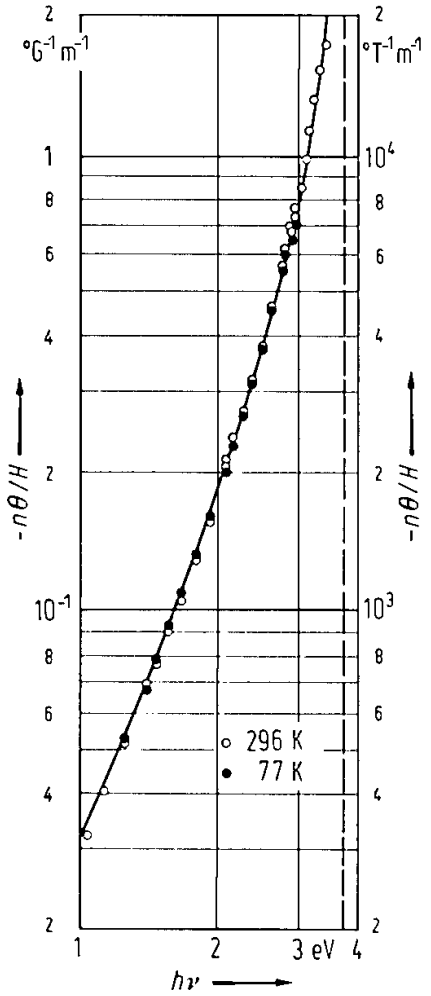

Fig. 1A-5-060. $KTaO_3$. $-n\theta/H$ vs. $h\nu$ [67Bae]. Parameter: *T*. *n*: refractive index, θ: Faraday rotation per unit length, *H*: magnetic field strength. Solid line: fit to dispersion function $F_1(\omega/\omega_g)$. See subsubsection 11. Dashed line: band gap energy E_g = 3.77 eV at 296 K, E_g = 3.79 eV at 77 K.

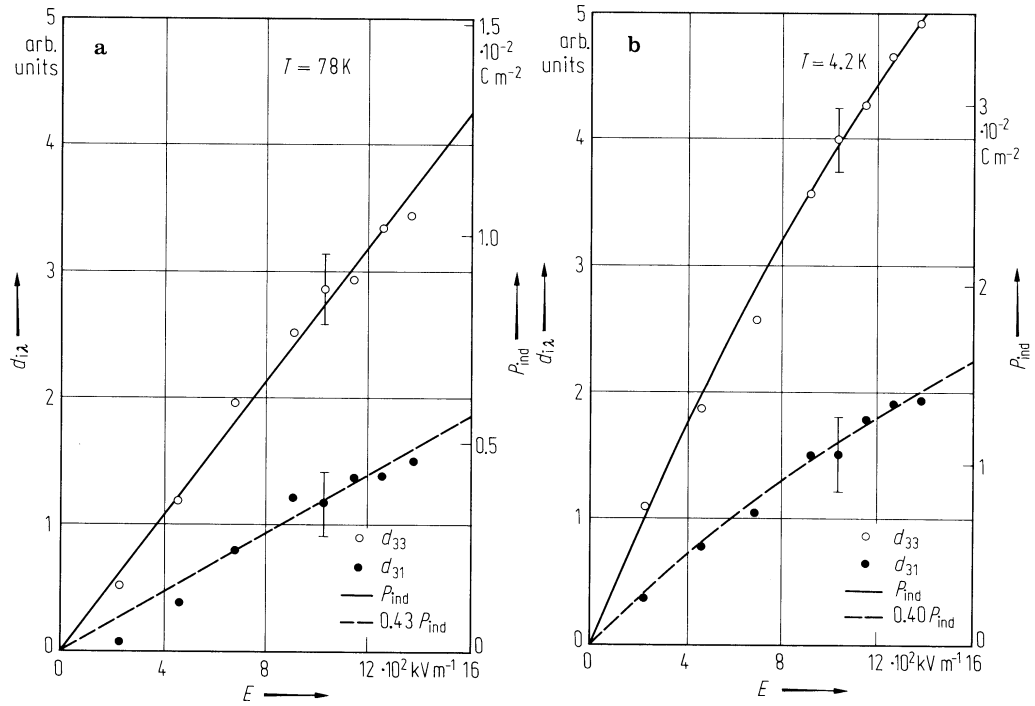

Fig. 1A-5-061. $KTaO_3$. $d_{i\lambda}$, P_{ind} vs. E [76Fuj2]. $d_{i\lambda}$: electric-field-induced nonlinear optical susceptibility, P_{ind}: induced polarization. **(a)** T = 78 K, **(b)** T = 4.2 K.

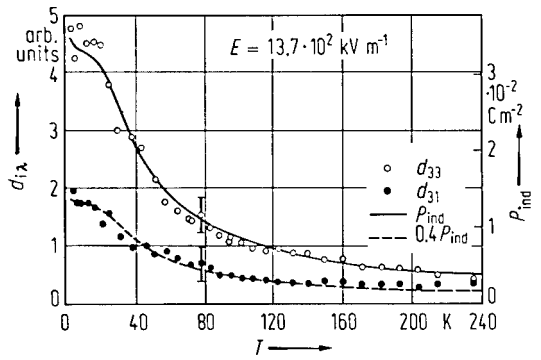

Fig. 1A-5-062. $KTaO_3$. $d_{i\lambda}$, P_{ind} vs. T [76Fuj2]. $d_{i\lambda}$: electric-field-induced nonlinear optical susceptibility, P_{ind}: induced polarization. $E = 13.7 \cdot 10^2$ kV m^{-1}.

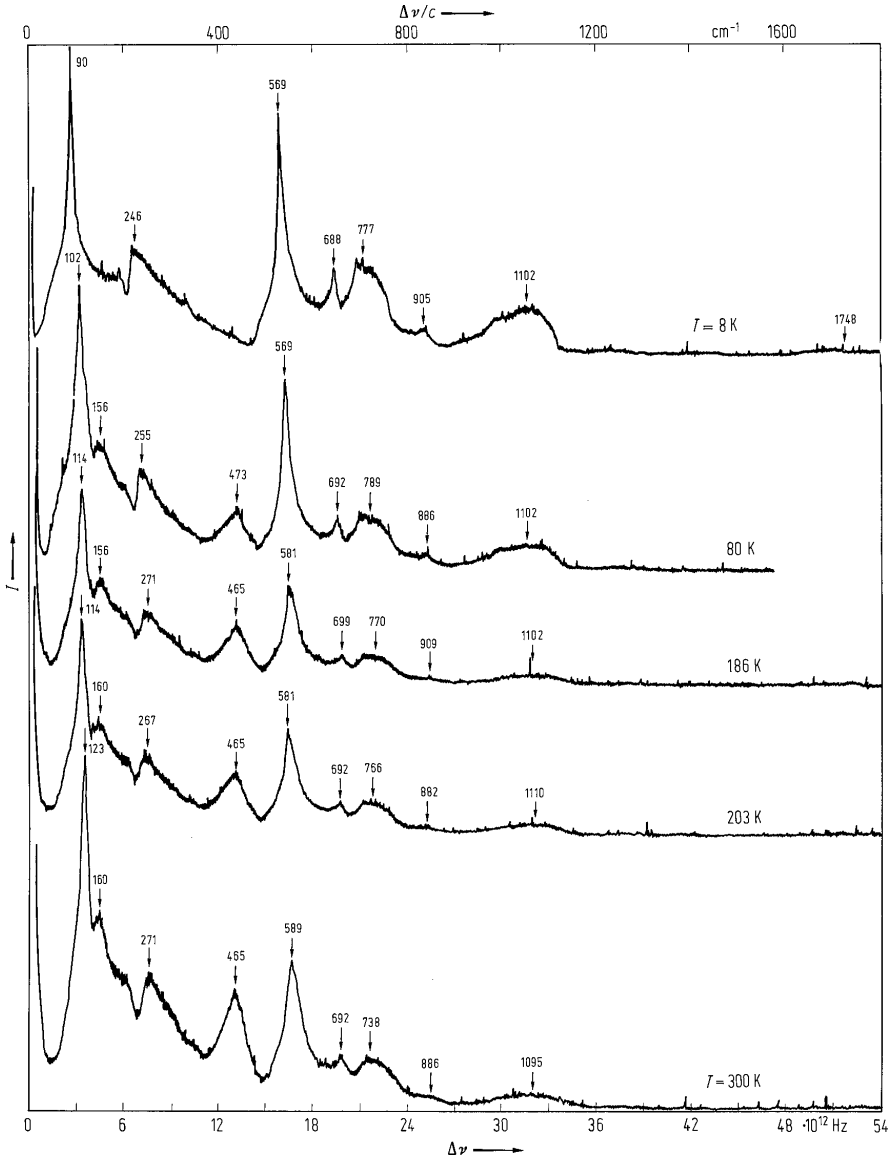

Fig. 1A-5-063. $KTaO_3$. I vs. $\Delta\nu$ [67Nil]. Parameter: T. I: Raman scattering intensity, $\Delta\nu$: frequency shift. Polarization geometry is $X(ZZ)Y$. Peak frequencies of the modes in the figure are given in units of cm^{-1}.

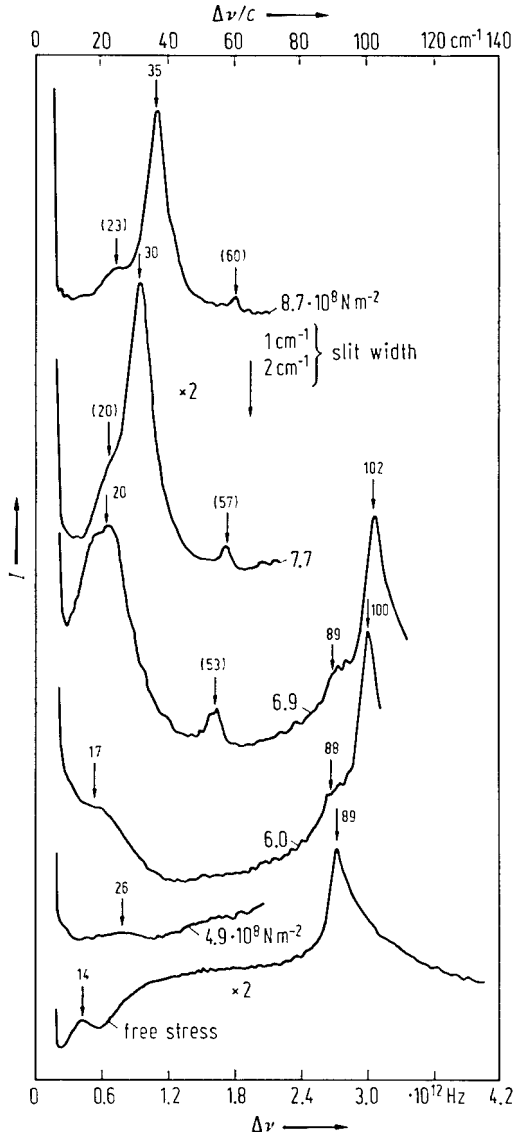

Fig. 1A-5-064. $KTaO_3$. I vs. $\Delta\nu$ [77Uwe]. I: Raman scattering intensity, $\Delta\nu$: frequency shift. Parameter: stress load along [010] (Y) axis. Scattering geometry is $XZ(YY)XZ$. Peak frequencies of the modes in the figure are given in units of cm^{-1}.

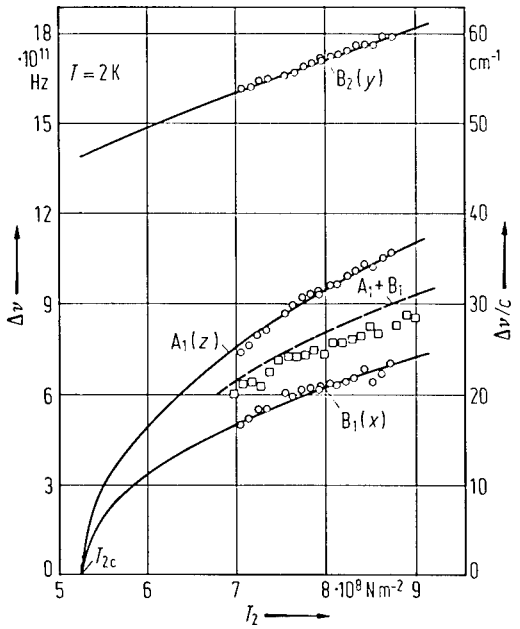

Fig. 1A-5-065. $KTaO_3$. $\Delta\nu$ vs. T_2 at 2 K [77Uwe]. $\Delta\nu$: Raman frequency shift, T_2: uniaxial stress parallel to *Y* axis. Solid lines represent the least square fit to data. The broken line is the calculated frequency for the mixed A_1+B_1 mode. T_{2c} = $5.25 \cdot 10^8$ Nm^{-2} is the estimated transition stress.

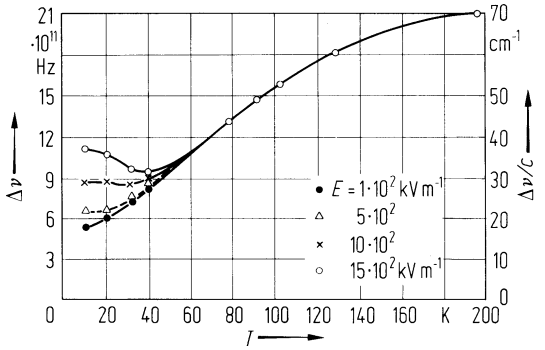

Fig. 1A-5-066. $KTaO_3$. $\Delta\nu$ vs. T [68Fle]. Parameter: electric field E. $\Delta\nu$: Raman frequency shift.

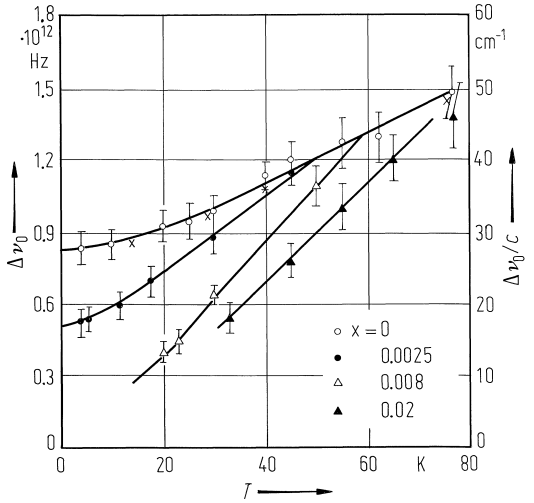

Fig. 1A-5-067. $KTa_{1-x}Nb_xO_3$. $\Delta\nu_0$ vs. T [81Pra2]. Parameter: x. $\Delta\nu_0$: Raman shift of the low frequency mode. Crosses: transverse acoustic (TA) mode frequency from theory. For x = 0.008, $\Theta_f \approx 17$ K. For x = 0.02, $\Theta_f \approx 28$ K.

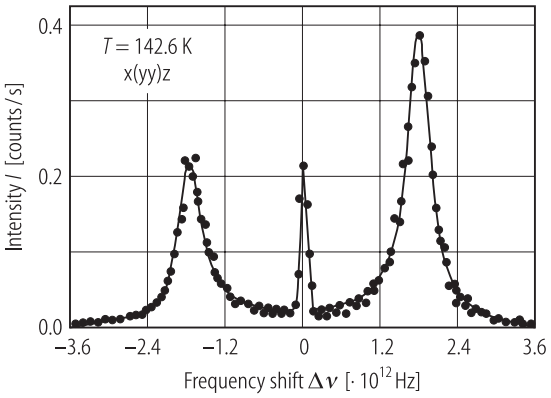

Fig. 1A-5-068. $KTaO_3$. I vs. $\Delta\nu$ [95Vog]. I: hyper-Raman scattering intensity. $\Delta\nu$: hyper-Raman frequency shift.

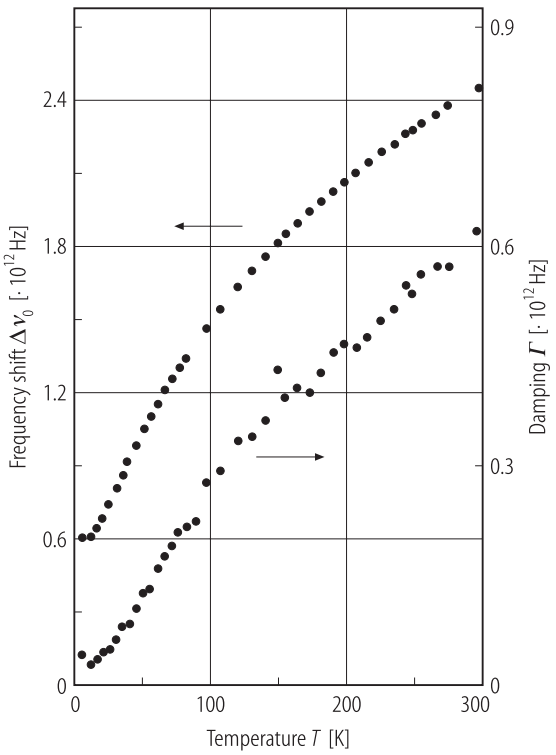

Fig. 1A-5-069. $KTaO_3$. $\Delta\nu_0$, Γ vs. T [95Vog]. $\Delta\nu_0$: soft mode frequncy. Γ: damping constant of the soft mode.

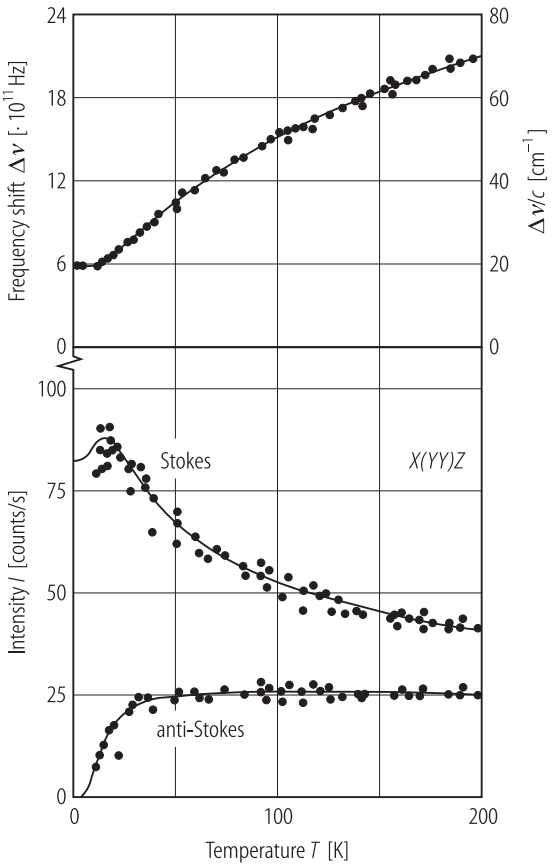

Fig. 1A-5-070. $KTaO_3$. $\Delta\nu$, I vs. T [90Vog]. $\Delta\nu$: soft mode frequency, I: hyper-Raman scattering intensity.

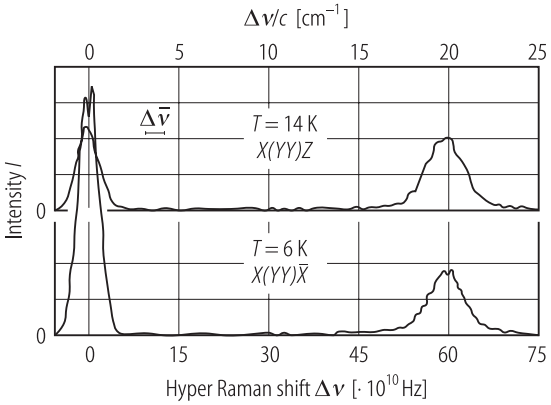

Fig. 1A-5-071. $KTaO_3$. I vs. $\Delta\nu$ [90Vog]. I: hyper-Raman scattering intensity of the X (YY) Z geometry at 14K (upper) and of the X (YY) $\overline{X}$ geometry at 6K. $\Delta\nu$: hyper-Raman frequency shift.

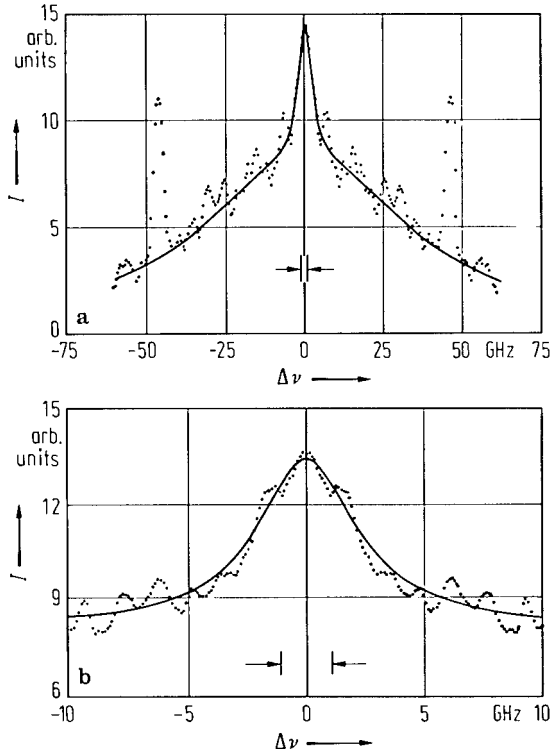

Fig. 1A-5-072. $KTaO_3$. I vs. $\Delta\nu$ [76Lyo]. I: intensity of the central peak. **(a)** Intensity of the central mode at 182 K, scattering angle is 90°. **(b)** More detailed spectrum of the central peak at 300 K, scattering angle is 135°.

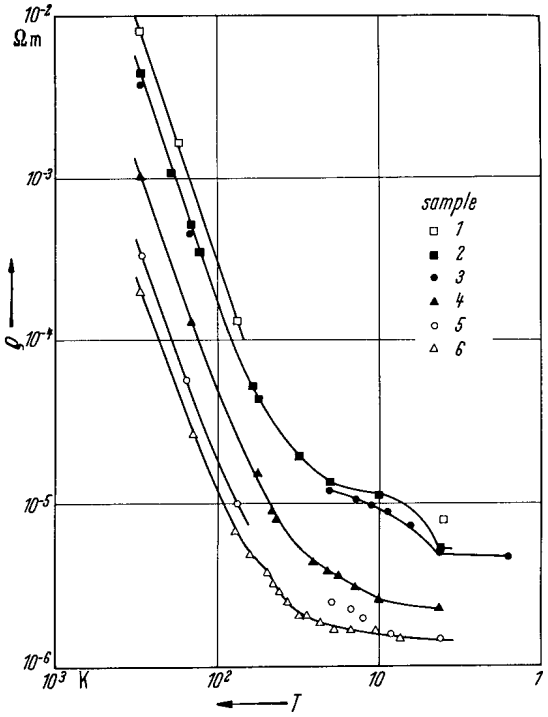

Fig. 1A-5-073. $KTaO_3$ (reduced). ρ vs. T for several samples of various carrier concentrations [65Wem]. See Table 1A-5-004 for the sample numbers and their carrier concentrations.

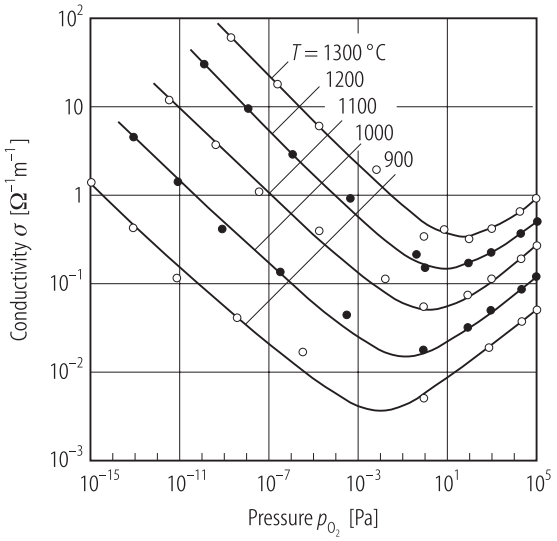

Fig. 1A-5-074. $KTaO_3$ (single crystal). σ vs. p_{O_2} [78Dep]. Parameter: T. p_{O_2}: oxygen partial pressure.

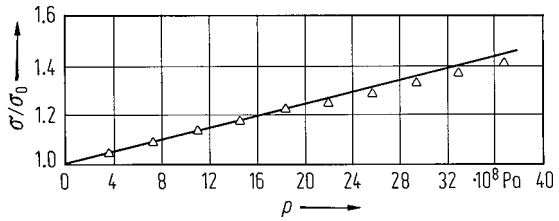

Fig. 1A-5-075. $KTaO_3$ (semiconducting). σ/σ_0 vs. p [66Wem]. σ_0: electrical conductivity for $p = 0$. Carrier concentration $N = (0.5...2)\cdot 10^{24}$ m^{-3}.

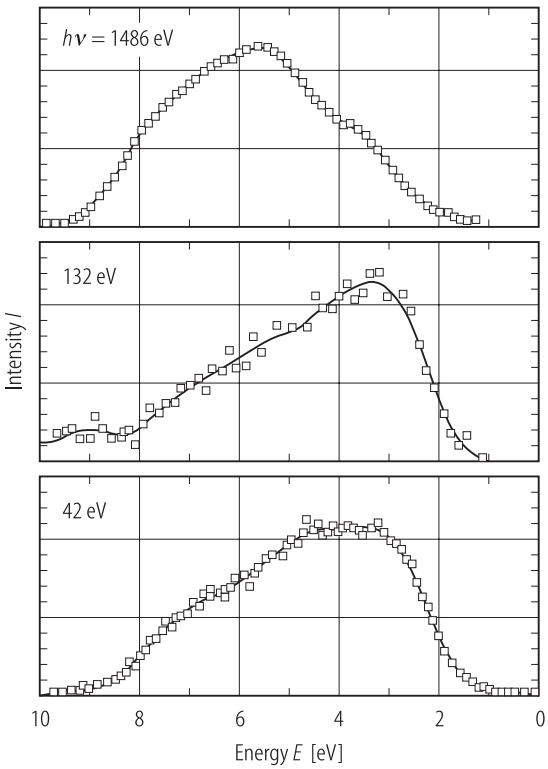

Fig. 1A-5-076. $KTaO_3$. X-ray photoelectron spectra for the valence band at RT [94Win]. Parameter: $h\nu$; photon energy of incident X-ray, monochromatized AlK α. *E*: binding energy below the valence band edge.

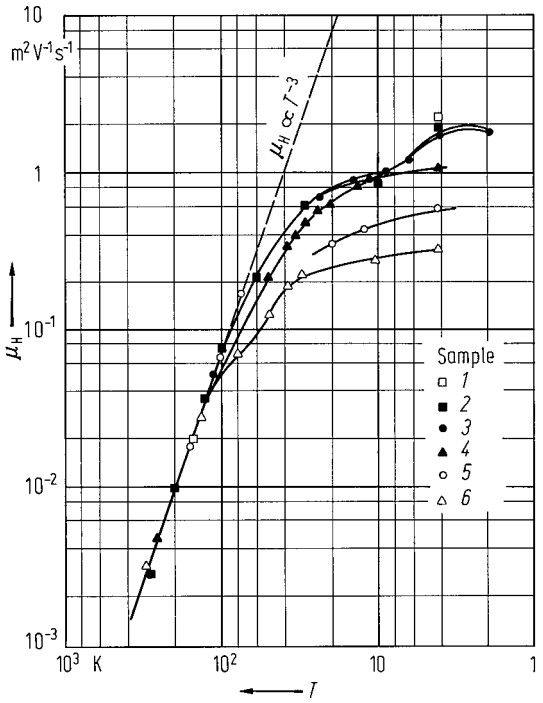

Fig. 1A-5-077. $KTaO_3$ (reduced). Hall mobility μ_H vs. T for single crystals with different concentrations [65Wem]. See Table 1A-5-004 for the sample numbers and their carrier concentrations.

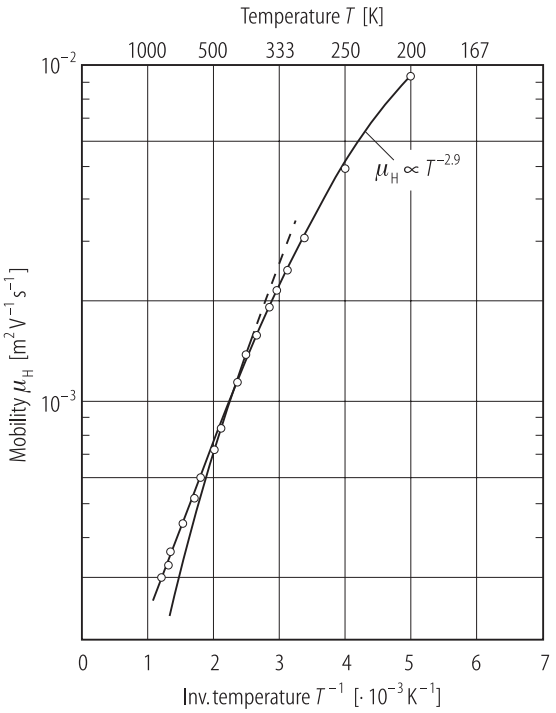

Fig. 1A-5-078. $KTaO_3$ (reduced). Hall mobility μ_H vs. $1/T$ [69Wem]. Solid curve: power-flaw fits to the data, dashed curve: exponential dependence $e^{\Theta/T}$, $\Theta \approx 1200$ K.

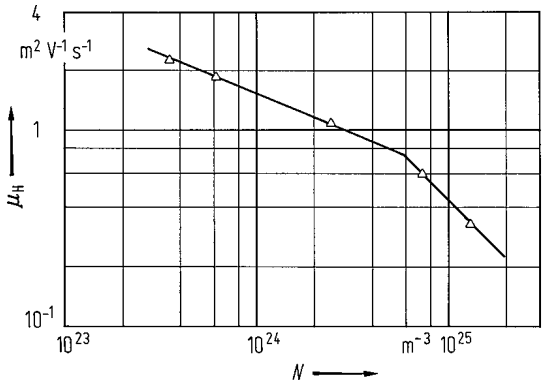

Fig. 1A-5-079. $KTaO_3$ (reduced). Hall mobility μ_H vs. carrier concentration N [65Wem]. T = 4.2 K.

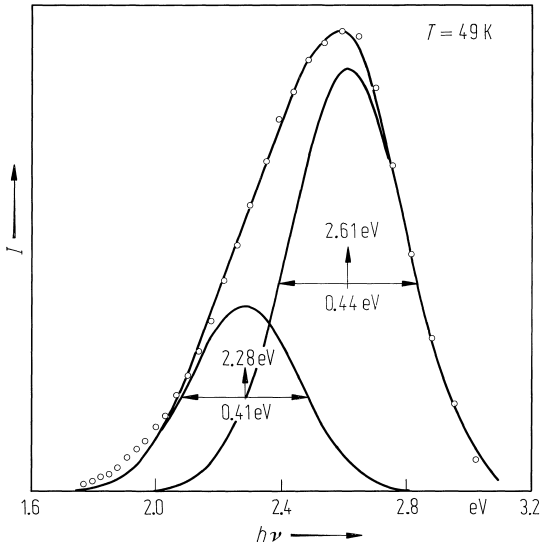

Fig. 1A-5-080. $KTaO_3$. *I* vs. $h\nu$ [87Yam]. *I:* luminescent emission intensity. For excitation, light with the band gap energy (≈ 4.0 eV) was used.

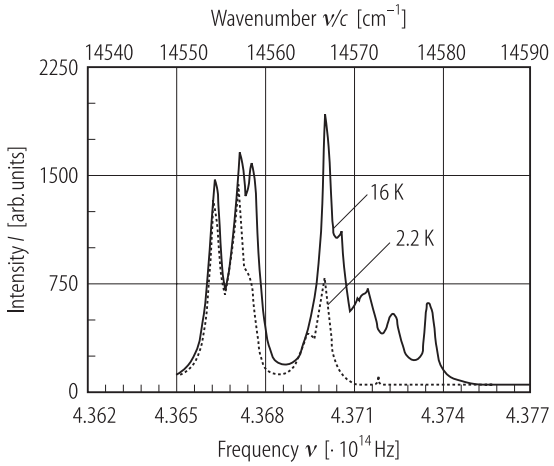

Fig. 1A-5-081. $KTaO_3$. *I* vs. ν [90Jan]. *I:* luminescent emmision intensity. Parameter: *T*.

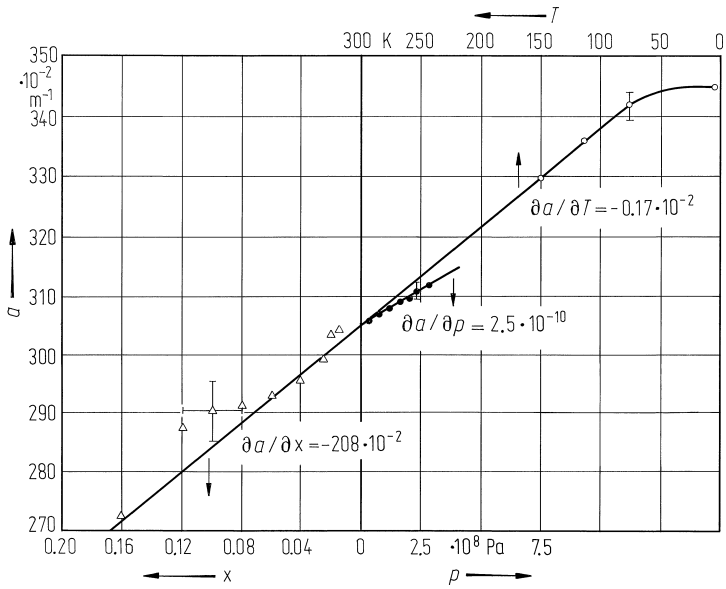

Fig. 1A-5-082. $KTaO_3$, $KTa_{1-x}Nb_xO_3$. *a* vs. *T* (open circles); *a* vs. *p* (full circles); *a* vs. x (open triangles) in $KTa_{1-x}Nb_xO_3$ [82Ryt]. *a*: cubic crystalline field splitting parameter of Fe^{3+}. *T*, *p* and x are calibrated with respect to the induced change of lattice parameter.

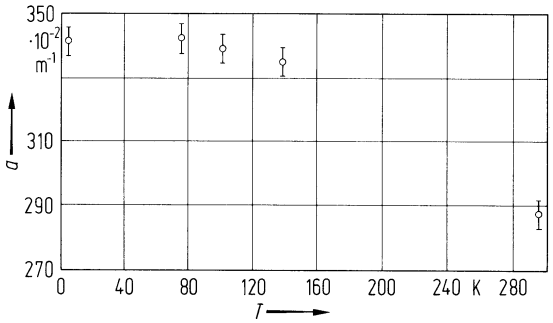

Fig. 1A-5-083. $KTaO_3$. *a* vs. *T* [67Han]. *a*: cubic crystalline field splitting constant of Fe^{3+} at the Ta^{5+} site.

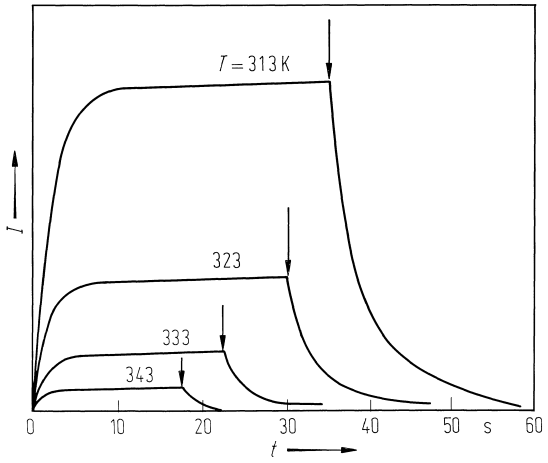

Fig. 1A-5-084. $KTaO_3$. Variation of ESR line intensity of Ni^{3+}–V_0–2e center with time, under blue light illumination [82Aki]. The arrows indicate the points where the illumination was terminated. Parameter: *T*.

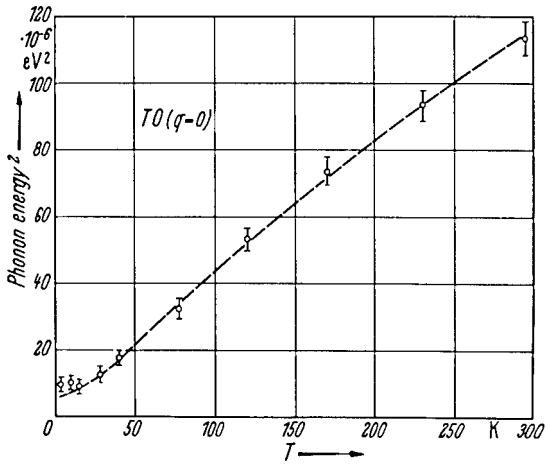

Fig. 1A-5-085. $KTaO_3$. Square of the phonon energy of the transverse optic mode at $q = 0$ (ferroelectric mode) vs. T [67Shi].

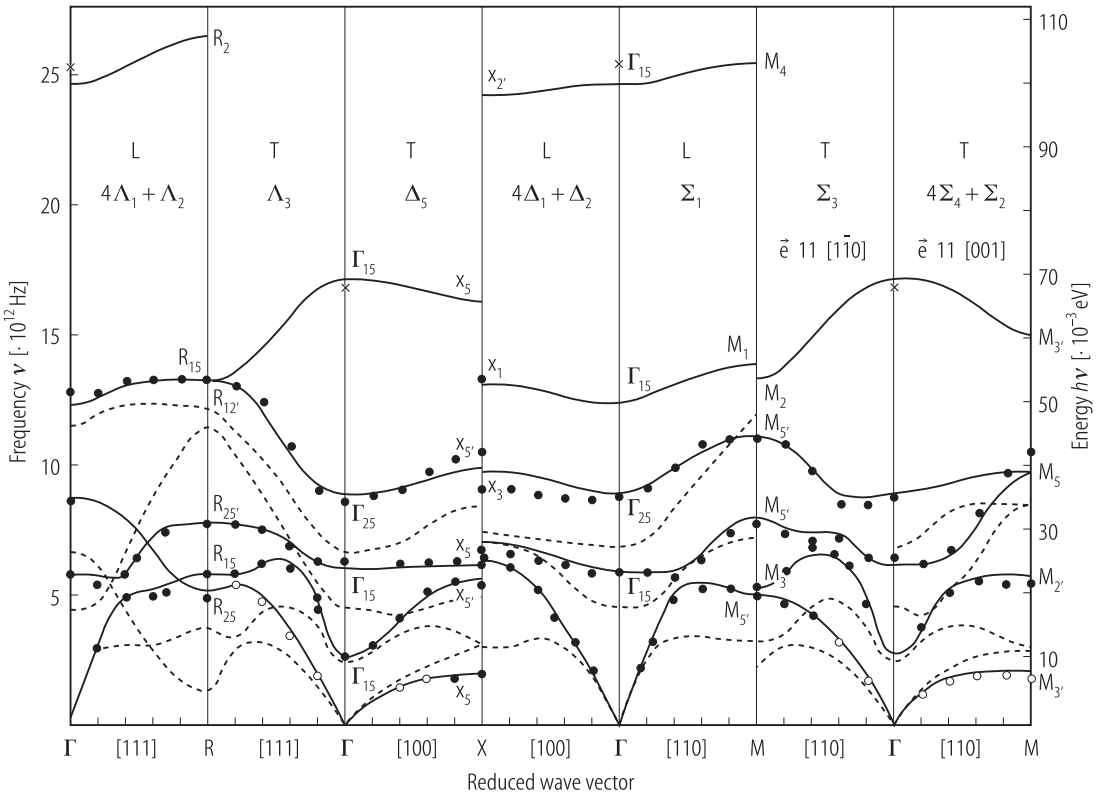

Fig. 1A-5-086. $KTaO_3$. Dispersion curves of inelastic neutron scattering [89Per]. ν: phonon frequency. T = 296 K. Full circles: data from [89Per], open circles: data from [72Com], crosses: data from infrared, Raman and hyper-Raman spectroscopy. Solid lines: fitting results. Dashed lines: measured dispersion curves for $SrTiO_3$ [72Sti, 76Sti].

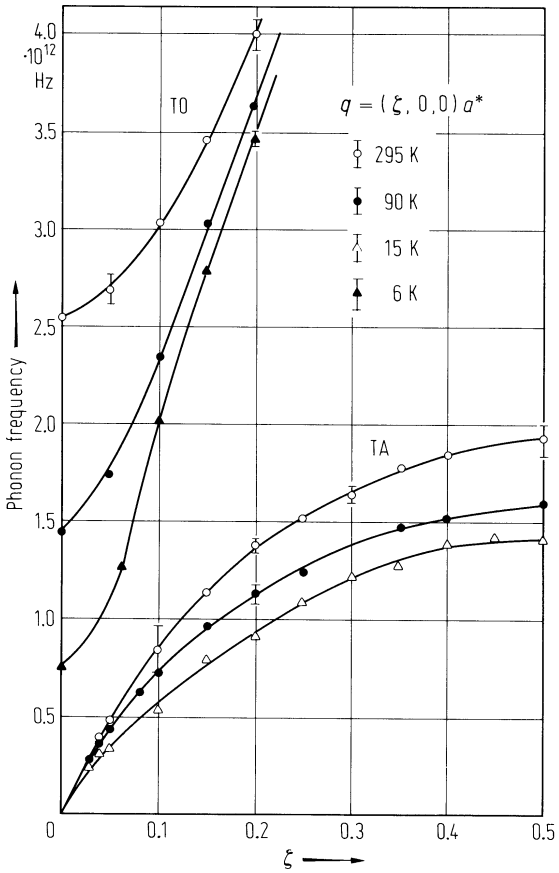

Fig. 1A-5-087. $KTaO_3$. Dispersion curves for (ζ, 0, 0) TA and soft TO phonons [70Axe]. Parameter: *T*.

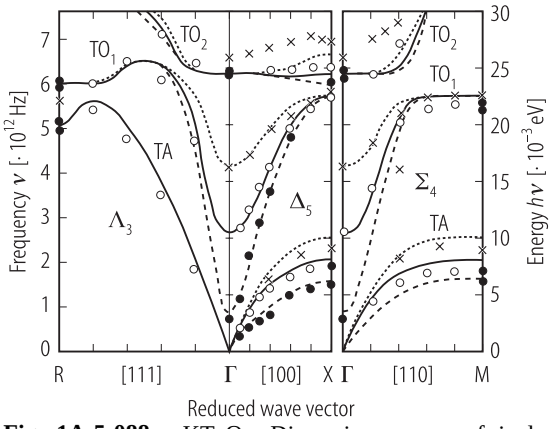

Fig. 1A-5-088. $KTaO_3$. Dispersion curves of inelastic neutron scattering [89Per]. Parameter: *T*. *ν*: phonon frequency. A part of data are taken from [67Shi, 70Axe, 72Com]. Dashed lines and full circles: T = 20 K, full lines and open circles: T = 296 K, dotted lines and crosses: T = 1220 K. The lines correspond to calculations.

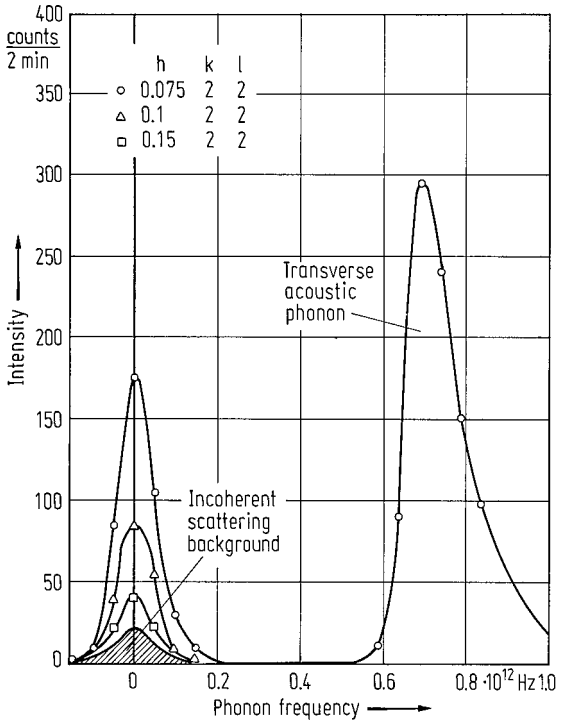

Fig. 1A-5-089. $KTaO_3$. Quasielastic neutron scattering found in the vicinity of the {100} sheets in reciprocal lattice [72Com]. Transverse acoustic phonon intensity is for comparison.

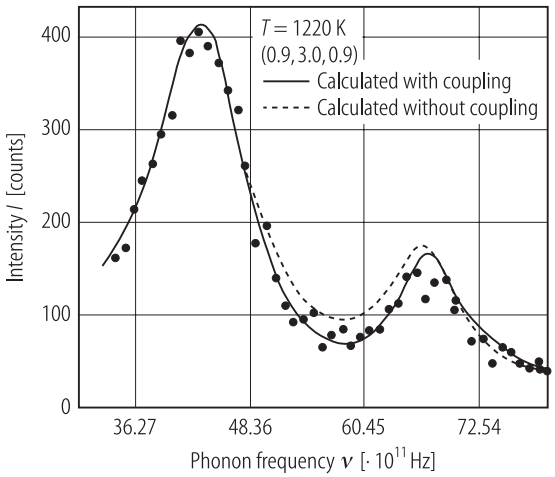

Fig. 1A-5-090. $KTaO_3$. Inelastic neutron scattering profile for the two lowest frequency transverse optic modes (TO_1 and TO_2) [89Per]. *I*: scattering intensity. *ν*: phonon frequency. Solid line and dashed line are profiles calculated with and without anharmonic coupling between the modes. The instrumental resolution width is indicated by the arrows.

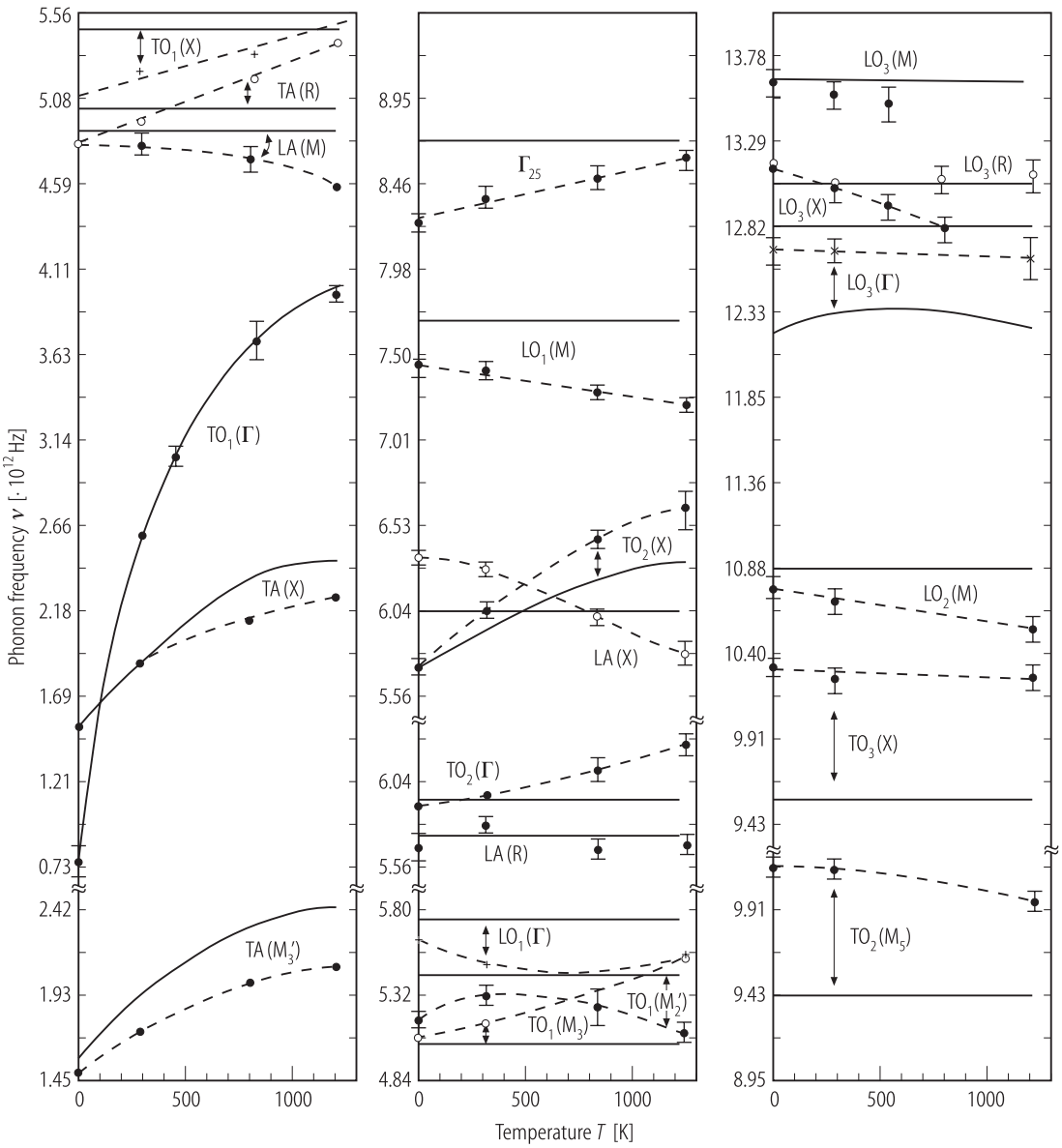

Fig. 1A-5-091. $KTaO_3$. Temperature dependence of zone-center and high-symmetry zone-boundary mode frequencies [89Per]. *ν*: phonon frequency. The dashed lines are guides to the eye for the experimental data. The solid lines are calculated from the model described in the original paper.